JACS
JOURNAL OF THE AMERICAN CHEMICAL SOCIETY

Article

pubs.acs.org/JACS

Sinefungin Derivatives as Inhibitors and Structure Probes of Protein Lysine Methyltransferase SETD2

Weihong Zheng,[†,⊥] Glorymar Ibáñez,[†,⊥] Hong Wu,[‡,⊥] Gil Blum,[†,§] Hong Zeng,[‡] Aiping Dong,[‡] Fengling Li,[‡] Taraneh Hajian,[‡] Abdellah Allali-Hassani,[‡] Maria F. Amaya,[‡] Alena Siarheyeva,[‡] Wenyu Yu,[‡] Peter J. Brown,[‡] Matthieu Schapira,[‡] Masoud Vedadi,[‡] Jinrong Min,*[,‡,∥] and Minkui Luo*[,†]

[†]Molecular Pharmacology and Chemistry Program, Memorial Sloan-Kettering Cancer Center, New York, New York 10065, United States

[‡]Structural Genomics Consortium, University of Toronto, 101 College Street, Toronto, Ontario, Canada M5G 1L7

[§]Tri-Institutional Training Program in Chemical Biology, Memorial Sloan-Kettering Cancer Center, New York, New York 10065, United States

[∥]Department of Physiology, University of Toronto, Toronto, Ontario, Canada M5S 1A8

Supporting Information

ABSTRACT: Epigenetic regulation is involved in numerous physiological and pathogenic processes. Among the key regulators that orchestrate epigenetic signaling are over 50 human protein lysine methyltransferases (PKMTs). Interrogation of the functions of individual PKMTs can be facilitated by target-specific PKMT inhibitors. Given the emerging need for such small molecules, we envisioned an approach to identify target-specific methyltransferase inhibitors by screening privileged small-molecule scaffolds against diverse methyltransferases. In this work, we demonstrated the feasibility of such an approach by identifying the inhibitors of SETD2. *N*-propyl sinefungin (Pr-SNF) was shown to interact preferentially with SETD2 by matching the distinct transition-state features of SETD2's catalytically active conformer. With Pr-SNF as a structure probe, we further revealed the dual roles of SETD2's post-SET loop in regulating substrate access through a distinct topological reconfiguration. Privileged sinefungin scaffolds are expected to have broad use as structure and chemical probes of methyltransferases.

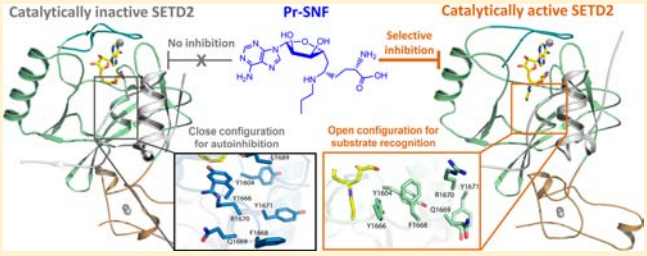

INTRODUCTION

Epigenetics involves heritable phenotypic changes that do not alter the genotype.[1,2] Among the essential epigenetic regulators are diverse post-translational modifiers such as protein lysine methyltransferases (PKMTs).[1−3] The human genome encodes more than 50 PKMTs, which use *S*-adenosylmethionine (SAM) as the cofactor and transfer its sulfonium methyl group to the ε-amino group of lysine side chains of specific protein substrates.[3] PKMT-mediated methylation regulates numerous biological functions, such as signal transduction, gene transcription, and protein stabilization.[1,2,4] The dysregulation of these events has been linked to various diseases, including cancer.[5,6] In view of the physiological and pathological relevance of the emerging epigenetic targets, there is an urgent need for small-molecule probes to investigate the biochemical properties of individual PKMTs and to manipulate them pharmacologically.[3,5,6]

With the exception of DOT1L, which contains a distinct catalytic domain,[7] PKMTs harbor a canonical 130 amino acid SET domain for SAM binding and enzymatic catalysis.[8−10] By exploiting the distinct SAM-binding motif of DOT1L, Daigle et al.[11] developed the SAM analogue EPZ004777 as a potent inhibitor of DOT1L with an in vitro half-maximal inhibitory concentration (IC_{50}) of 0.3 nM. The difference between DOT1L and other PKMTs also allowed Yao et al.[12] to design 5′-aziridine-based SAM analogues as DOT1L-selective inhibitors. Apart from the rational design approach, medium- or high-throughput screening led to the identification of inhibitors of SET-domain PKMTs, such as chaetocin for *Drosophila melanogaster* SU(VAR)3−9 (likely human SUV39H1), BIX-01294 for G9a (likely its homologue GLP), and AZ505 for SMYD2.[3,13−15] However, the handful of inhibitors cannot satisfy the increased need for PKMT chemical probes directed toward understanding the epigenetic roles of more than 50 human PKMTs.[3] Since most PKMTs rely on the highly conserved SET domain for SAM binding and less-structured regions for substrate recognition, it seems challenging to develop PKMT inhibitors with both selectivity and potency in a rational manner.[3] In this work, we envisioned an approach to screen diverse methyltransferases against privileged small-molecule scaffolds to identify target-specific PKMT inhibitors.

Received: July 19, 2012
Published: October 8, 2012

dx.doi.org/10.1021/ja307060p | *J. Am. Chem. Soc.* 2012, 134, 18004−18014

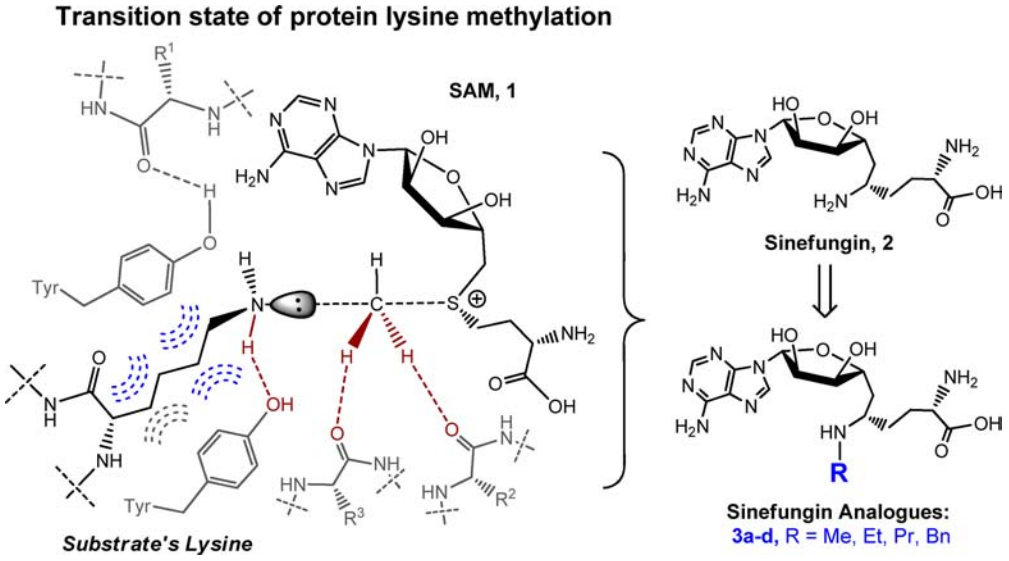

Figure 1. Structures of a proposed transition state of protein lysine methylation and sinefungin analogues as the transition-state mimics. The transition state features classical hydrophobic interactions/hydrogen bonds with the lysine side chain of the substrate and nonclassical C−O hydrogen bonds with the sulfonium methyl moiety of SAM. Sinefungin (**2**) and its analogues **3a−d** are expected to capture certain transition-state characters of specific PKMTs.

Scheme 1. Synthesis of Sinefungin Analogues 3a−d

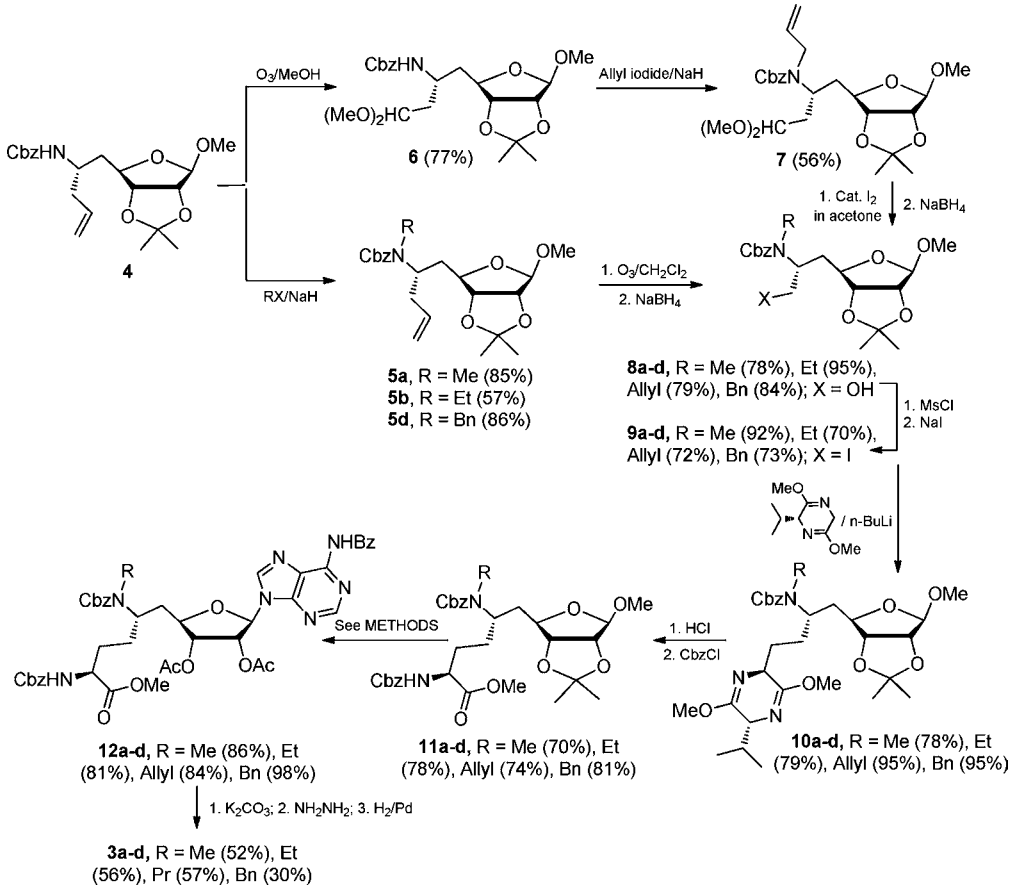

Enzymatic transition-state theory argues that even closely related enzymes may adopt distinct transient structures along the reaction path of enzymatic catalysis and thus could be selectively inhibited by structurally matched small molecules.[16,17] Molecular dynamics modeling and static structures of PKMTs suggest that transition-state stabilization at substrate−cofactor interfaces of PKMTs involves both classical hydrophobic interactions/hydrogen bonds with the lysine side chain of substrates and nonclassical C−O hydrogen bonds with the sulfonium methyl moiety of SAM (Figure 1).[18,19] Here we envisioned the development of *N*-alkyl sinefungins as PKMT inhibitors by capturing certain transition-state characters

dx.doi.org/10.1021/ja307060p | J. Am. Chem. Soc. 2012, 134, 18004−18014

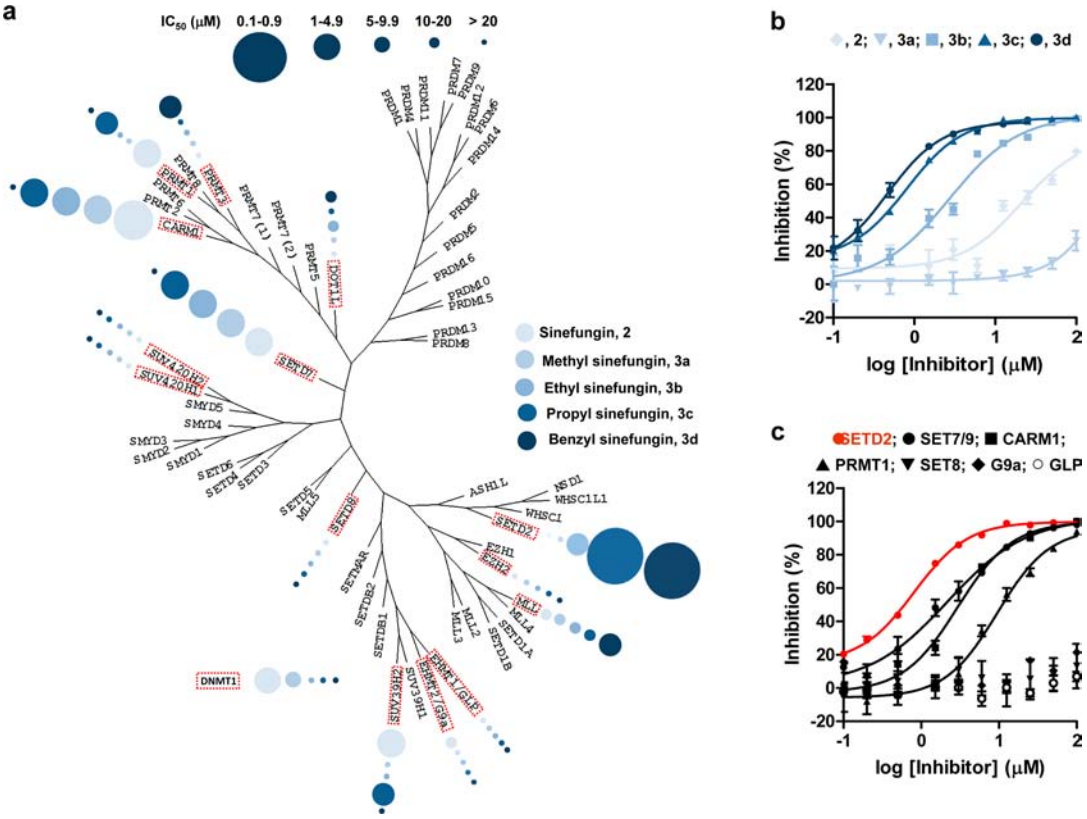

Figure 2. Inhibition profile of sinefungin and its analogues **3a**−**d** against a panel of methyltransferases. (a) The magnitude of IC_{50} of sinefungin and its analogues **3a**−**d** is presented against 15 phylogenetically arrayed methyltransferases (their IC_{50} values are listed in Table S1). The increased diameters and darkness of the circles reflect higher potency (lower IC_{50}) and larger sizes of the inhibitors, respectively. (b) Representative IC_{50} curves of sinefungin and its analogues **3a**−**d** against SETD2 with the values of 28.4 ± 1.5, >100, 8.2 ± 1.2, 0.80 ± 0.02, and 0.48 ± 0.06 μM for sinefungin and **3a**−**d**, respectively. (c) IC_{50} curves of Pr-SNF **3c** against representative methyltransferases with the values of 0.80 ± 0.02 μM for SETD2, 2.2 ± 0.4 μM for SET7/9, 3.0 ± 0.3 μM for CARM1, 9.5 ± 0.4 μM for PRMT1, >100 μM for SET8, G9a, and GLP.

(Figure 1). To achieve high affinity to specific PKMTs, such sinefungin analogues are expected to position their secondary amines at the substrate−cofactor interface and the *N*-alkyl chains at the lysine-binding pocket for optimal interactions (Figure 1).

Human SETD2 is a tumor-suppressing PKMT implicated in p53-dependent gene regulation, transcription elongation, and intron−exon splicing.[20−26] Aberrant activities of SETD2 and its homologues NSD1/2/3 have also been implicated in various developmental syndromes and cancers.[20,27−32] Here we report that *N*-alkyl sinefungin analogues act as SETD2-specific inhibitors by matching distinct transition-state characters of SETD2. With the aid of *N*-propyl sinefungin (Pr-SNF, **3c**; Figure 1), we further revealed that the post-SET loop of SETD2 goes through a remarkable reconfiguration for inhibitor binding, substrate recognition, and enzymatic catalysis. Since structurally diverse sinefungin variants can be examined in a similar manner, the sinefungin-based scaffolds are expected to display broad utility as structure or pharmacological probes of protein methyltransferases.

■ RESULTS

Synthesis of Sinefungin Analogues 3a−d. With sinefungin as a privileged small-molecule scaffold to screen PKMT inhibitors, sinefungin analogues **3a**−**d** were prepared from the reported D-ribose derivative **4** (Scheme 1).[33] To access *N*-alkyl (alkyl = methyl, ethyl, benzyl) analogues **3a**, **3b**, and **3d**, the common precursor **4** was alkylated with the corresponding haloalkanes (methyl/ethyl iodide, benzyl bromide) to afford **5a**, **5b**, and **5d**, respectively. In contrast to the ready alkylation of **4** to **5a**, **5b**, and **5d**, the reaction of **4** with iodopropane was sluggish (<15% yield), likely because of the low reactivity of the haloalkane. To circumvent this problem and achieve the preparation of **3c**, we adopted an alternative strategy involving ozonolysis of the terminal alkene of **4** followed by Me_2S workup in the presence of methanol to yield **6**,[34] which was then alkylated using more reactive allyl iodide to furnish **7** (the allyl group served as the precursor of Pr-SNF's *N*-propyl moiety). Primary alcohols **8a**−**d** were obtained via ozonolysis of terminal-alkene-containing **5a**, **5b**, and **5d** and I_2-facilated acetal deprotection of **7**,[35] followed by hydride reduction. Mesylation of **8a**−**d** and subsequent iodination afforded **9a**−**d**. The chiral amino acid moiety of **3a**−**d** was introduced using the Schöllkopf bis-lactim ether chiral auxiliary in the synthesis of **10a**−**d**.[36,37] These intermediates were processed into **11a**−**d** and then **12a**−**d** after hydrolytic removal of the pyrazine and isopropylidene, protection of the amino moiety with a benzyloxycarbonyl (Cbz) group, acetylation of the ribosyl hydroxyl moieties, and then incorporation of N^6-benzoyladenine under Vorbrüggen conditions.[33] Further conversion of **12a**−**d** by sequential treatments with K_2CO_3 (to remove acetates), hydrazine (to remove the methyl ester and N^6-benzoyl group), and Pd-catalyzed hydrogenolysis (to remove Cbz selectively and reduce the allyl group) yielded the desired final products **3a**−**d** in overall yields of 7−11% from **4** (Scheme 1; also see the Supporting Information).

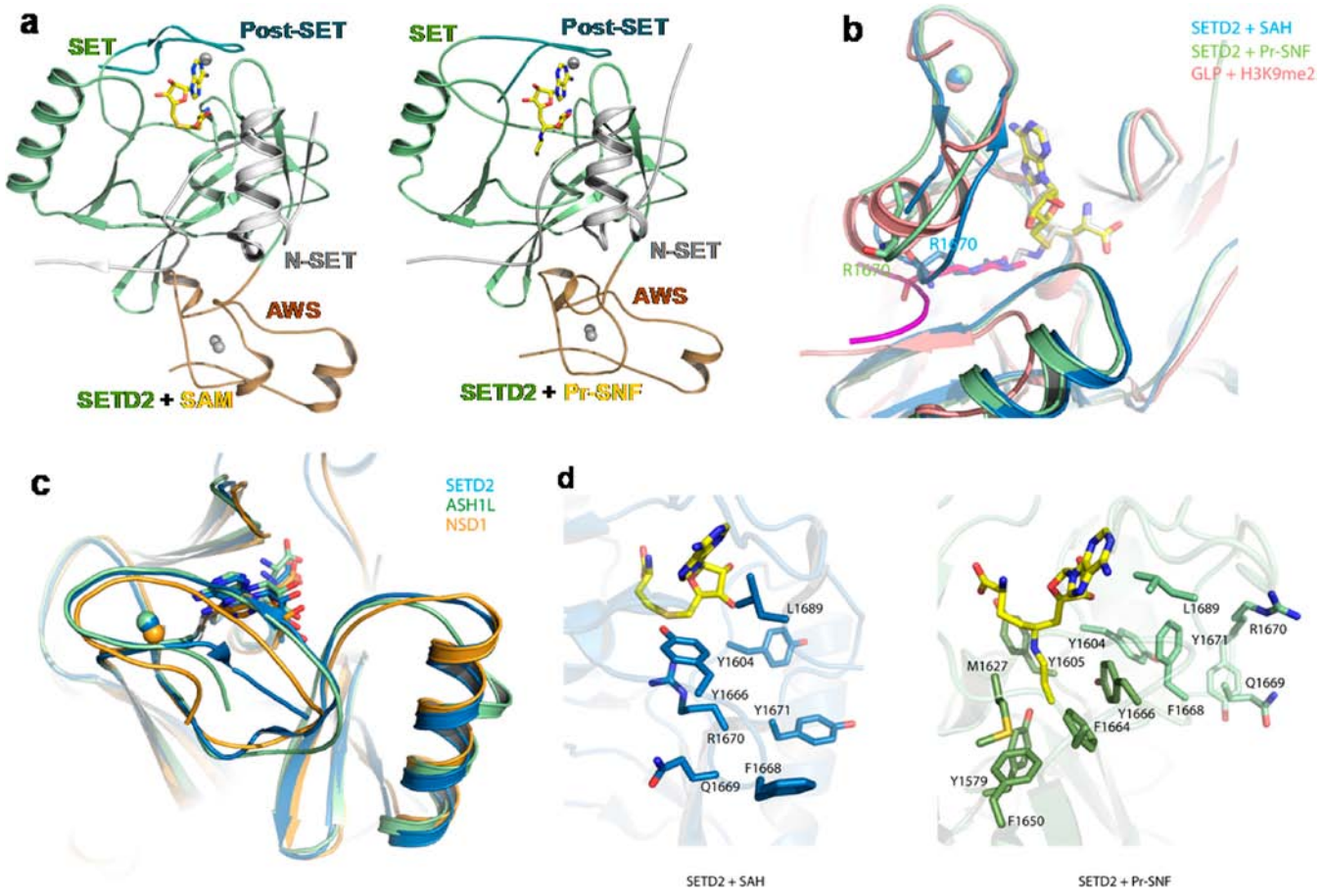

Figure 3. Structures of SETD2 in complex with SAH and Pr-SNF. (a) Overall crystal structures of SETD2 in complex with SAH (left) and Pr-SNF **3c** (right). Here the catalytic domain of human SETD2 (residues 1435−1711) contain the N-terminal extension motif, AWS domain (orange), SET domain (light green), and post-SET motif (cyan) with the ligands (SAH or Pr-SNF) highlighted. (b) Superposition of the binary complexes of SAH−SETD2 (blue-yellow, PDB code 4H12), Pr-SNF−SETD2 (green-white, PDB code 4FMU), and H3K9me2−GLP (mauve-magenta, PDB code 2RFI). Overlaid structures between SAH−SETD2 and H3K9me2−GLP show that the autoinhibitory loop in the SAH−SETD2 complex and its R1670 (blue) bind the site that would be otherwise occupied by the substrate (magenta) of GLP. In contrast, the loop and its characteristic R1670 are repositioned in the structure of Pr-SNF−SETD2 (green) and overlaid with the post-SET helix (mauve) for binding substrate. (c) Superposed structures of the inactive binary complex SAH−SETD2 (blue, PDB code 4H12) and its homologues, ASH1L (green, PDB code 3OPE) and NSD1 (orange, PDB code 3OOI). The three PKMTs have the similar autoinhibitory topology with their post-SET loops. (d) The key residues to stabilize the alternative configuration of the post-SET loop and interact with Pr-SNF's *N*-propyl chain. In the SETD2−Pr-SNF (right) but not SETD2−SAH (left) binary complex, SETD2's post-SET loop is glued at a hydrophobic core consisting of Tyr1604, Tyr1666, Phe1668, Leu1689, and the hydrocarbon side chain of Arg1670. In the SETD2−Pr-SNF, the *N*-propyl moiety was buried in the hydrophobic binding pocket formed by SETD2's Tyr1579, Tyr1605, Met1627, Phe1650, Phe1664, and Tyr1666.

Pr-SNF (3c) and *N*-Benzyl Sinefungin (3d) as Potent, Selective Inhibitors of SETD2. With sinefungin and its derivatives **3a−d**, we examined their inhibition profile against a panel of human methyltransferases, including 10 SET-domain PKMTs (SET7/9, SET8, EZH2, MLL, GLP, G9a, SUV39H2, SETD2, SUV420H1, and SUV420H2) as well as 5 non-SET-domain PKMTs (PRMT1, PRMT3, CARM1, DOT1L, and DNMT1) (Figure 2). Among the 5 × 15 panel of small molecules and enzymes, **3c** (Pr-SNF) and **3d** displayed 2−200- and 10−100-fold preferences, respectively, to SETD2 over other examined methyltransferases (Figure 2a and Table S1). The potency of **3c** and 3**d** against SETD2 (apparent IC_{50} of 0.8 ± 0.2 and 0.48 ± 0.06 μM, respectively) is more than 10-fold higher than that of sinefungin **2**, **3a**, and **3b** (Figure 2b and Table S1). This structure−activity relationship (SAR) indicated that the *N*-propyl/benzyl moieties of **3c** and **3d**, in contrast to the free amine of sinefungin **2** and *N*-methyl/ethyl groups of **3a** and **3b**, contribute to the tight interaction with SETD2. For other examined methyltransferases in the 5 × 15 assay panel against **3a−d**, only SET7/9 and CARM1 show modest μM range IC_{50} of 1.4−3.0 μM, which are not significantly different from IC_{50} of the parent compound sinefungin **2**, a pan-methyltransferase inhibitor (Figure 2c and Table S1).[3] With the exception of SETD2 among the examined 15 methyltransferases, appending the small alkyl moieties (e.g., methyl/ethyl/propyl groups) to sinefungin deteriorates or has no effect on its IC_{50} (Table S1). In contrast, the strong preference of **3c** and **3d** against SETD2, together with their well-correlated SAR, presents the two sinefungin derivatives as SETD2-specific inhibitors with decent potency and selectivity.

Pr-SNF as a Structure Probe Specific for SETD2's Active Conformer. To elucidate the molecular mechanism of the potency and selectivity of the sinefungin derivatives as SETD2 inhibitors, we solved the structures of the binary complexes of SETD2's catalytic domain (AWS, SET, and post-SET motifs) with *S*-adenosyl-L-homocysteine (SAH, which was

dx.doi.org/10.1021/ja307060p | *J. Am. Chem. Soc.* 2012, 134, 18004−18014

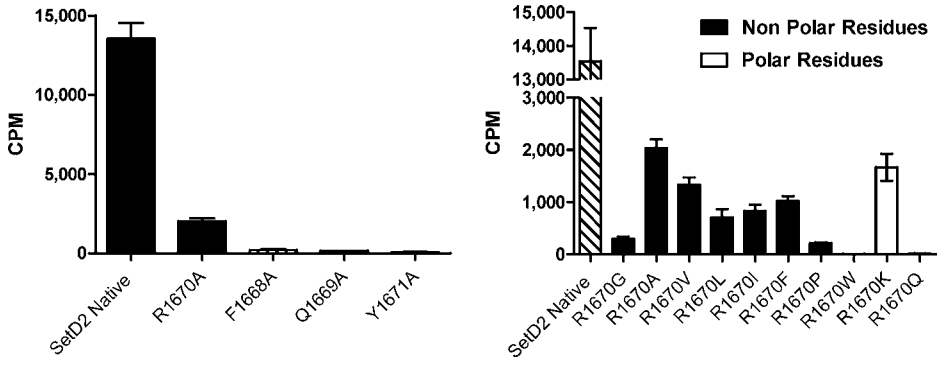

Figure 4. Effects of SETD2's enzyme catalysis. Methylation activities of SETD2 and its mutants were measured through the filter paper assay with [^{3}H-Me]-SAM as cofactor. The F1668A, Q1669A, R1670G/A/V/L/I/F/P/W/K/Q, and Y1671A mutations are within SETD2's post-SET loop, which regulates substrate access. The barely detectable methylation activities of SETD2's F1668A. Q1669A and Y1671A mutants are consistent with their roles on either stabilizing SETD2's active open conformer or interacting with substrate. SETD2's 1670 site can tolerate modest hydrophobic substitutions (e.g., A/V/I/L/F) but not extreme ones (e.g., G/P/W).

degraded from SAM under the crystallization condition, Methods section) and Pr-SNF **3c** (Figure 3a). In the presence of SAH, SETD2 adopts a compact configuration with its AWS motif and post-SET motif interwoven with the central SET domain. The SAH molecule is located within a deep pocket formed between SETD2's SET and post-SET domains, as conserved among all known SET-domain PKMTs (e.g., SET7/9, SET8, G9a, GLP, MLL, SUV39H2, SUV420H1, and SUV420H2).[9,38,39] However, the SETD2−SAH binary complex is distinct by its autoinhibitory post-SET loop, which is positioned to prevent substrate binding, and its characteristic Arg1670 residue located in the pocket that is otherwise occupied by substrate lysine (Figure 3b). Such autoinhibitory topology has also been reported for NSD1 and ASH1L, two closely related homologues of SETD2, and proposed to regulate the access of substrates to the PKMTs (Figure 3c, S2).[10,40−42]

Although the overall structure of the binary complex of SETD2 with Pr-SNF **3c** is similar to that with SAH, a remarkable difference was revealed at the post-SET motif of SETD2 in complex with Pr-SNF (Figure 3b,d). The overlaid structures of SETD2 with Pr-SNF and SAH showed that the Pr-SNF's propyl group partially extends into the lysine-binding pocket (Figure 3b,d). To accommodate this *N*-propyl moiety, which would otherwise clash with the Arg1670 residue in the SETD2−SAH complex, SETD2 orients this arginine 15 Å away from the lysine-binding pocket by flipping the otherwise autoinhibitory post-SET loop (Figure 3d). This reconfiguration also vacates SETD2's catalytic site for the entry of substrates (this site is occupied by the post-SET loop in the SETD2−SAH complex). To stabilize this substrate-accessible configuration in the SETD2−Pr-SNF binary complex, SETD2's post-SET loop is glued at a newly formed hydrophobic core through Tyr1604, Tyr1666, Phe1668, Leu1689, and the hydrocarbon side chain of Arg1670 (Figure 3d). The structure overlay with the substrate-bound GLP further revealed that Gln1669/Tyr1671 in the SETD2's post-SET loop and the helix between SETD2's Glu1588−Asn1599 region are topologically comparable to GLP's Arg1214/Ile1218 and GLP's Ser1132−Glu1138 helix region (Figure 3b).[43,44] Given that these residues of GLP play the key role on substrate recognition,[43,44] the comparable regions of SETD2 (Gln1669/Tyr1671 in the post-SET loop; the helix of aa 1588−1599) are expected to participate in substrate binding in a similar manner. Comparing the overlaid structures of Pr-SNF−SETD2 and SAH−SETD2 also revealed a 45° rotation of Tyr1666 residue, although its biological relevance remains unknown. Collectively, these results showed that SETD2's methyltransferase domain can adopt at least two alternative conformations through flipping its post-SET loop: an autoinhibitory close conformation and a substrate-accessible open conformation. Here Pr-SNF **3c** plays a key role as a structure probe through its preferential interaction with the latter.

Effects of Mutations of SETD2's Post-SET Loop on Enzyme Catalysis. Structural analysis of SETD2 underscored the importance of SETD2's post-SET loop to receive substrate. To confirm the role of SETD2's post-SET loop, we mutated SETD2's F1668, Q1669, R1670, and Y1671 residues to alanine (Figure 4). The barely detectable methylation activities of SETD2's F1668A and Q1669A/Y1671A mutants are consistent with their proposed roles in stabilizing SETD2's active open conformer and interacting with substrate, respectively. In contrast, SETD2's R1670A mutant partially retains the methylation activity. To further examine the role of this residue in enzyme catalysis, Arg1670 was systematically replaced with nonpolar/hydrophobic amino acids G/V/I/L/P/F/W as well as polar amino acids K/Q. The overall activity profile indicated that SETD2's Arg1670 site can tolerate modest (e.g., A/V/I/L/F) but not extreme hydrophobic substitutions (e.g., G/P/W) (Figure 4). This observation is consistent with the role of the hydrocarbon portion of Arg1670s side chain to stabilize SETD2's active open conformer by interacting with the nearby hydrophobic core. Such interaction is expected to be partially maintained by replacing the arginine with certain hydrophobic residues (Figure 3d). The complete loss of activity of SETD2's R1670Q mutant versus partial loss of the activity of the R1670K/A/V/I/L/F mutant also suggests that both the charge and the hydrophobic side chain of SETD2's Arg1670 play certain roles on the enzyme catalysis (Figure 4). These mutagenesis results therefore confirm the roles of SETD2's post-SET loop and its Arg1670 on substrate interaction, as revealed above by SETD2's structures.

Characterization of Pr-SNF as a SETD2 Inhibitor via Enzyme Kinetics. The structure of the Pr-SNF−SETD2 binary complex suggests that, to accommodate Pr-SNF, SETD2 needs to adopt the catalytically active open configuration with its post-SET loop aligned for substrate entry. Given the present

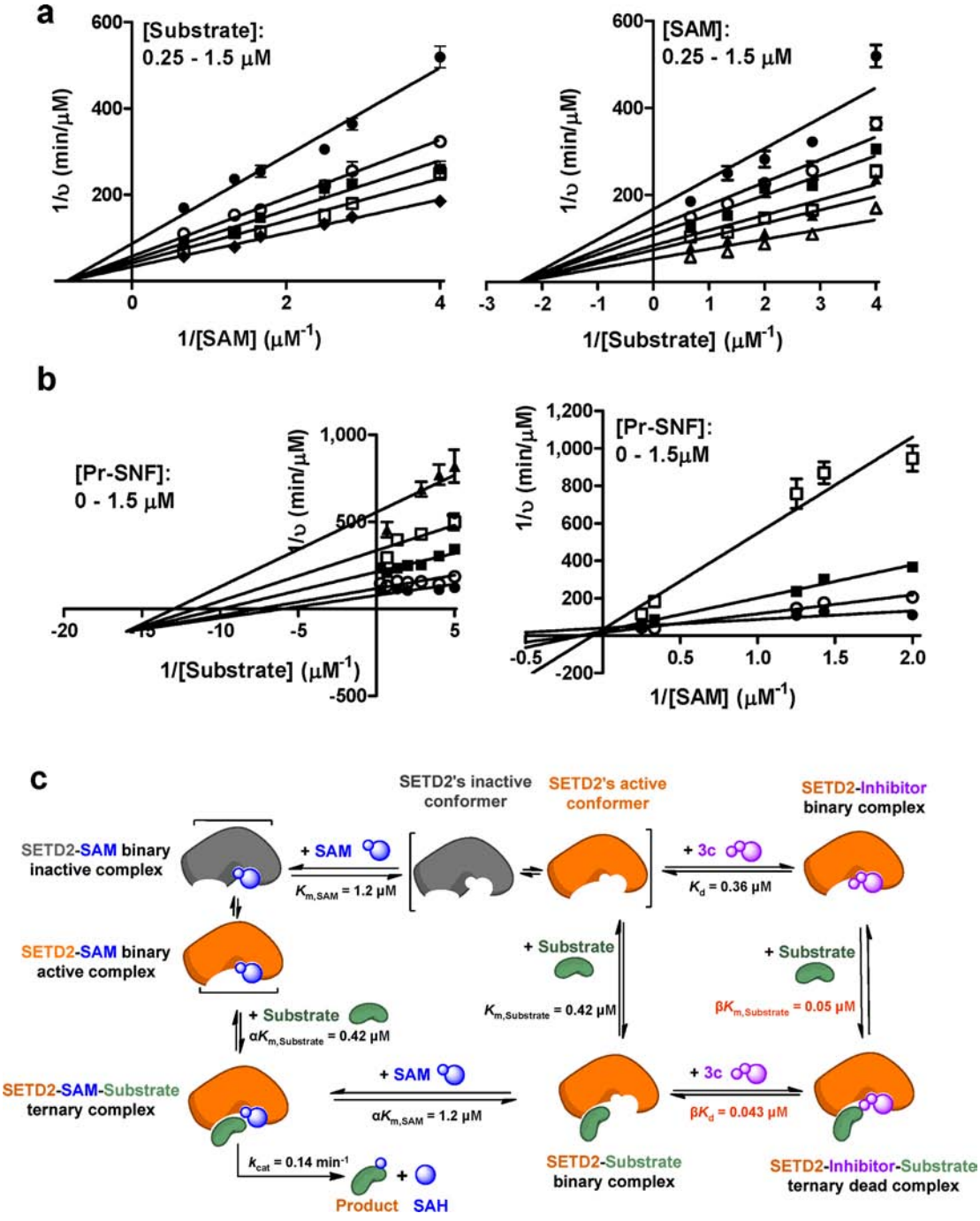

Figure 5. Methylation kinetics of SETD2. The kinetic analysis was carried out with varied concentrations of substrate and cofactor in the absence (a) or presence (b) of Pr-SNF. (a) Initial velocities for SETD2-mediated methylation were measured to generate the Lineweaver−Burk curve versus the concentration of the SAM cofactor (0.25−1.5 μM) (left) or the concentration of the H3K36 peptide substrate (0.25−1.5 μM) (right). The linear regressions, which converge on the x axis in both cases, suggest a random sequential mechanism. $K_{m,SAM}$ = 1.21 ± 0.05 μM, $K_{m,Substrate}$ = 0.42 ± 0.02 μM, α = 1, and k_{cat} = 0.14 ± 0.1 min^{-1} were obtained by plotting the slopes of the Lineweaver−Burk double reciprocal curves against the concentrations of SAM and substrate (Figure S1a and SI). (b) Double reciprocal plots of initial velocities of SETD2-mediated methylation versus the concentration of substrate or SAM in the presence of Pr-SNF (0−1.5 μM) were generated by varying the concentration of substrate (0.25−5 μM) (left) in the presence of the fixed concentration of SAM (0.8 μM) or by varying the concentration of cofactor (0.5−4 μM) in the presence of the fixed concentration of the substrate (4 μM) (right). The linear regressions, converging on the negative x axis against substrate and on the y axis against SAM, are consistent with a noncompetitive mechanism between Pr-SNF and substrate and a competitive mechanism between Pr-SNF and SAM. K_d = 360 ± 15 nM and βK_d = 43 ± 4 nM (β = 0.12 ± 0.01) were obtained by plotting the slopes of the double reciprocal curves against the concentration of Pr-SNF (Figure S1b and SI). (c) Overall mechanisms and kinetic parameters of SETD2-mediated methylation in the absence or presence of Pr-SNF. SETD2-mediated methylation goes through a random sequential mechanism and can be inhibited by Pr-SNF via forming either the Pr-SNF−SETD2 binary or the Pr-SNF−SETD2−substrate ternary complexes.

difficulty to obtain the structure of the SETD2−substrate complex, such topological switch was validated through analyzing the kinetics of SETD2-catalyzed methylation in the absence or presence of Pr-SNF (Figure 5). The initial velocities

dx.doi.org/10.1021/ja307060p | J. Am. Chem. Soc. 2012, 134, 18004−18014

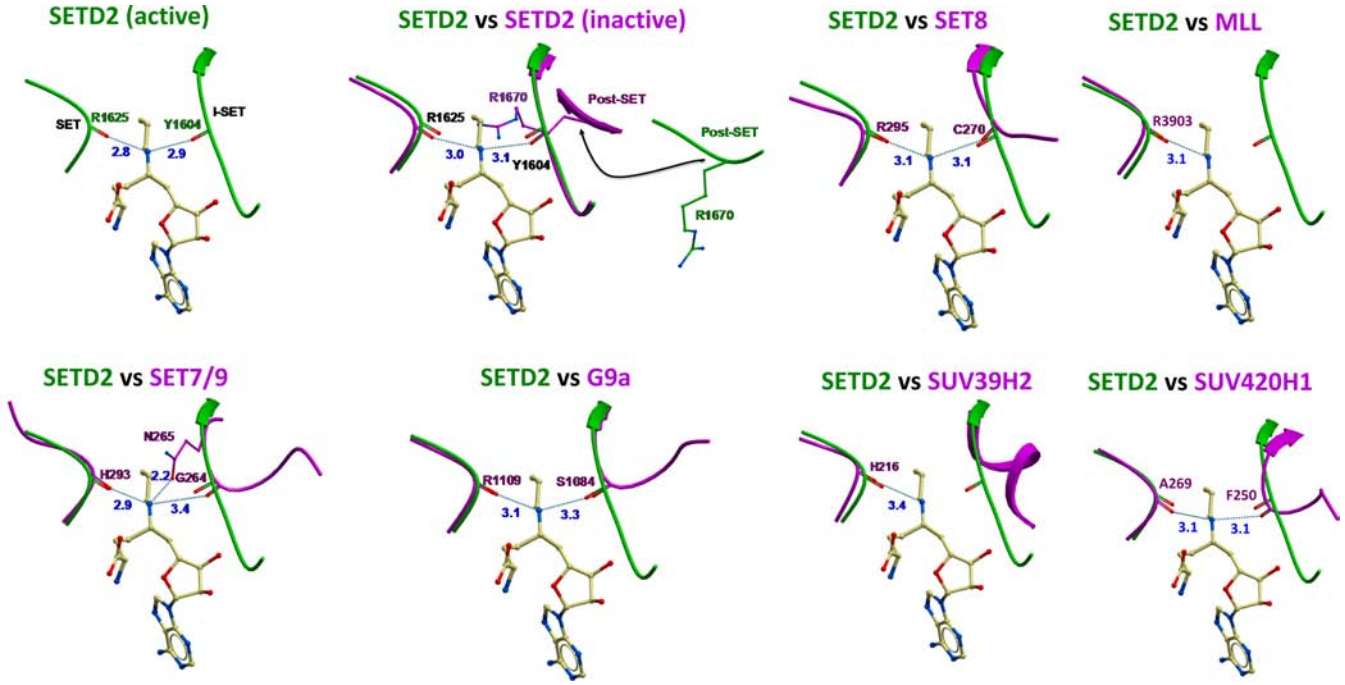

Figure 6. Structural insights of Pr-SNF's selectivity on SETD2 over other PKMTs. Pr-SNF ligand in the Pr-SNF−SETD2 binary complex (PDB code 4FMU) was overlaid with SAM or SAH in complex with SET7/9 (PDB code 1O9S), SETD2's autoinhibitory conformer (PDB code 4H12), SET8 (PDB code 1ZKK), MLL (PDB code 2W5Z), G9a (PDB code 3RJW), GLP (PDB code 2RFI), SUV39H2 (PDB code 2R3A), SUV420H1 (PDB code 3S8P), and SUV420H2 (PDB code 3RQ4) with ICM version 3.7-2b (Molsoft, San Diego). The overlaid structures of GLP and SUV420H2 were omitted given their similarity to those of G9a and SUV420H1, respectively. The optimal hydrogen-bonding distances between Pr-SNF's secondary amine and main-chain carbonyls observed in the SETD2 structure may contribute to the high selectivity of the inhibitor.

of SETD2-catalyzed methylation were monitored with the H3 peptide (20−50 amino acid) as H3K36 substrate and [^{3}H-Me]-SAM as cofactor. The plots of the initial velocities versus concentrations of peptide substrate or SAM cofactor were first generated in the absence of Pr-SNF. The linear regression did not converge on the y axis (Figure 5a) and thus ruled out an ordered sequential mechanism: the ordered SAM/substrate or substrate/SAM binding along the reaction path of SETD2-catalyzed methylation.[45] The converged initial velocities on the x axis versus the concentrations of peptide substrate or SAM further argue that SETD2-catalyzed methylation goes through a random sequential mechanism, and the binding of either SAM or substrate does not affect the sequential binding of the other (α = 1, Figure 5c).[45] Plotting the slopes of the double reciprocal kinetics against the concentrations of SAM or substrate gives SETD2's $K_{m,SAM}$ of 1.21 ± 0.05 μM, $K_{m,Substrate}$ of 0.42 ± 0.02 μM, and k_{cat} = 0.14 ± 0.1 min^{-1} (Figure 5c, S1a). The similar results were obtained via nonlinear regression of the same set of kinetic data (Figure S1b).

To accurately determine the dissociation constant K_d of **3c** on SETD2, we measured initial velocities of SETD2-catalyzed methylation versus concentrations of peptide substrate and SAM cofactor as the function of the concentration of Pr-SNF **3c**. In the presence of the varied amount of **3c** and the fixed amount of SAM, the double-reciprocal kinetics of SETD2-catalyzed methylation versus peptide substrate converged in the negative region of x axis (Figure 5b left).[45] This result implicated a noncompetitive character between Pr-SNF and peptide substrate, featured as coexistence of the inhibitor−enzyme binary and inhibitor−enzyme−substrate ternary complexes (Figure 5c).[45] Given that Pr-SNF's *N*-propyl moiety and the H3K36 lysine chain could clash if simultaneously occupying SETD2's lysine-binding pocket, the formation of the inhibitor−enzyme−substrate complex is intriguing and can be better elucidated upon solving the structure of the ternary complex.

The converged linear regression in the negative region of y axis further revealed that the initial binding of either Pr-SNF **3c** or substrate facilitates the following binding of the other (β < 1) (Figure 5b, left and c). In contrast, in the presence of the varied amount of Pr-SNF and the fixed amount of peptide substrate, the double-reciprocal kinetics of SETD2-catalyzed methylation versus SAM cofactor converged on y axis, consistent with the competitive character between Pr-SNF **3c** and SAM cofactor (Figure 5b, right and c). Upon fitting these kinetics with $K_{m,SAM}$ = 1.21 ± 0.05 μM, $K_{m,Substrate}$ = 0.42 ± 0.02 μM, and α = 1, K_d = 360 ± 15 nM, and βK_d = 43 ± 4 nM (β = 0.12 ± 0.01) were obtained for Pr-SNF to bind SETD2 in the absence and presence of substrate, respectively (Figures 5c and S1b). These values are consistent with the IC_{50} of **3c** against SETD2 as measured with sub-K_m concentrations of SAM cofactor and peptide substrate (calculated IC_{50} of 0.60 μM versus experimental IC_{50} of 0.80 μM shown in Figure 2). Our kinetic data together with SETD2's structures thus concluded that SETD2-catalyzed methylation goes through a random sequential mechanism and that Pr-SNF **3c** inhibits this process through the formation of either a Pr-SNF−SETD2 binary complex or a Pr-SNF−SETD2−substrate ternary complex (Figure 5c). The small β value of 0.12 further argues that the binding of Pr-SNF to SETD2 significantly facilitates the subsequent recruitment of substrate to form the inhibitor−SETD2−substrate ternary dead complex ($K_{m,Substrate}$ = 0.42 ± 0.02 μM versus $\beta K_{m,Substrate}$ = 0.050 ± 0.005 μM, Figure 5c). The high affinity of the Pr-SNF−SETD2 binary complex to

dx.doi.org/10.1021/ja307060p | J. Am. Chem. Soc. 2012, 134, 18004−18014

substrate peptide, as reflected by small $\beta K_{m,Substrate}$ of 0.050 ± 0.005 μM, also recapitulates the prior finding that **3c** preferentially interacts with SETD2's active open conformer and thus position SETD2's post-SET loop in a ready configuration to bind substrate.

Selective Inhibition of Pr-SNF 3c on SETD2 versus Other SET-Domain PKMTs. To further explore the origin of the selectivity of Pr-SNF **3c** on SETD2 versus other SET-domain PKMTs, we superimposed SETD2-bound Pr-SNF to SAM or SAH in complex with SETD2's autoinhibitory close conformer and other PKMTs. The secondary amine of Pr-SNF **3c** is expected to be protonated at physiological pH and thus carries two hydrogen atoms. In SETD2's active open conformation, Pr-SNF's secondary amine moiety is ideally positioned to form the two hydrogen bonds with the backbone carbonyl of SETD2's R1625 and Y1604 (N−O distances of 2.8 and 2.9 Å, respectively) (Figure 6). The comparable carbonyl groups of SET7/9 have also been proposed to participate in transition-state stabilization and enzymatic catalysis at the substrate−cofactor interface by forming nonclassic oxygen−carbon hydrogen bonds with SAM's sulfonium methyl moiety.[18] In contrast, such carbonyl residues in SETD2's inactive conformer (SETD2 in complex with SAH) and the prior SET domain structures (e.g., SET8, MLL, GLP, G9a, SUV39H2, SUV420H1, and SUV420H2) are not well positioned with the less optimally docked N−O distances of >3.1 Å for the carbonyl groups (Figures 3 and 6). In these cases, the formation of the optimal hydrogen bonds would require the PMTs to alter ground-state conformations and thus pay additional energy penalty. Despite the near-optimal N−O distances of 3.1 Å in the structures of SETD8, SUV420H1, and SUV420H2 (Figure 6), Pr-SNF shows even lower affinity in contrast to MLL and SUV39H2 (Table S1). This observation indicates that additional factors may further contribute to the altered affinity of Pr-SNF on PKMTs. In the case of SET7/9, the amide oxygen of the side-chain of N265 can form an alternative hydrogen bond, which may compensate the less optimal carbonyl hydrogen bond and thus cause the modest cross-inhibition observed (Figures 2 and 6). This analysis therefore suggests that SETD2's active open conformer contains the two well-positioned backbone carbonyls to form the hydrogen bonds with Pr-SNF, and these interactions in part account for its selective inhibition on SETD2 over other PKMTs.

Here we further argue that the *N*-propyl moiety of Pr-SNF also plays a positive role on its preferential interaction with SETD2's active open conformer, because sinefungin and its *N*-methyl derivative **3a** do not show such selectivity (Table S1). In the structure of the SETD2−Pr-SNF binary complex, Pr-SNF's *N*-propyl moiety was located in the hydrophobic binding pocket of substrate lysine formed by SETD2's Tyr1579, Tyr1605, Met1627, Phe1650, Phe1664, and Tyr1666 (Figure 3d). The readiness of the lysine-binding pocket to accommodate *N*-alkyl groups is thus essential for Pr-SNF's selectivity on SETD2. Here SETD2's lysine-binding pocket can be explored with the *N*-alkyl sinefungin analogues **3a**−**d** as structure probes (Figure 2 and Table S1). The gradually reduced IC_{50} of 100, 8.2 ± 1.2, 0.80 ± 0.20, and 0.48 ± 0.06 μM from **3a**−**d** on SETD2 indicates that the lysine-binding pocket of SETD2 is flexible enough to accommodate bulky propyl or benzyl moiety. In contrast, 10−50-fold drop in potency from **3c** to **3d** suggests that the lysine-binding pockets of SET7/9 and SUV39H2 are not sufficient for **3d**'s benzyl group. These findings therefore substantiate the importance of the matched lysine-binding pocket, besides the two well-positioned backbone carbonyls (Figure 6), for Pr-SNF's selectivity on SETD2 over other PKMTs.

■ DISCUSSION

Synthesizing the privileged *N*-alkyl sinefungin derivatives and screening them against a panel of methyltransferases allowed us to identify Pr-SNF **3c** and *N*-benzyl sinefungin **3d** as inhibitors of SETD2. Among the examined 10 SET domain PKMTs (SET7/9, SET8, EZH2, MLL, GLP, G9a, SUV39H2, SETD2, SUV420H1, and SUV420H2) and 5 non-SET domain methyltransferases (PRMT1, PRMT3, CARM1, DOT1L, and DNMT1), Pr-SNF **3c** and *N*-benzyl sinefungin **3d** showed the best inhibition on SETD2 with apparent IC_{50} of sub-μM (K_d = 0.36 ± 0.02 μM for Pr-SNF). Further characterization of Pr-SNF revealed that the presence of SETD2's substrate enhances its K_d by additional 8-fold (βK_d = 0.043 ± 0.004 μM). SETD2 is solely responsible for H3K36 trimethylation and has been characterized as a tumor suppressor of multiple cancers.[22,24,46] Here we present Pr-SNF **3c** (likely *N*-benzyl sinefungin **3d** as well) as a SETD2-specific inhibitor.

Pr-SNF was further demonstrated to be a valuable structure probe of human SETD2. Pr-SNF **3c** preferentially interacts with SETD2's catalytically active open conformer. Compared with SETD2's autoinhibitory close conformer, the active open conformer is featured by a distinct reconfiguration of a post-SET substrate-recognizing loop. In particular, SETD2's Arg1670 residue plays dual roles by orienting the loop to block the substrate entry in the inactive close conformer but readily receive the substrate in the active open conformer. The configuration switch also positions SETD2's backbone carbonyl groups to form two optimal hydrogen bonds with Pr-SNF's secondary amine. The presence of Pr-SNF **3c** therefore favors the equilibrium to SETD2's catalytically active open conformer. Remarkably, NSD1 and ASH1L were also reported to contain similar autoinhibitory loops to prevent free access of substrates.[40−42,47] SETD2, NSD1, and ASH1L are more closely related among the SET-domain-containing PKMTs on the basis of their primary sequence (Figure S2) and their ability to recognize H3K36 as a substrate.[40−42,47] The autoinhibitory topology may be adapted by the subfamily of PKMTs as a general mechanism to regulate substrate recognition. The switch from the autoinhibitory to catalytically active configuration of the subfamily of PKMTs could be modulated by their binding partners in cellular contexts and thus account for their context-specific substrate recognition.[48]

Pr-SNF's preference for SETD2 over 14 other methyltransferases is striking given the overall structural similarity between the 10 examined SET-domain-containing PKMTs.[38,39] Structural analysis and enzyme kinetics of SETD2, together with the results of mutagenesis and molecular docking, indicated that such selectivity relies on the existence of the matched lysine-binding pocket and unique catalytically active conformer of SETD2. To rationally design inhibitors of protein methyltransferases, several prior efforts focused on conjugating a portion of substrates to a 5′-azo-SAM analogue (bisubstrate-type inhibitors).[3,12,49,50] With exception of the 5′-aziridine-based inhibitor of DOT1L, whose structural topology is different from other protein methyltransferases,[12] most bisubstrate-type inhibitors only showed modest IC_{50}.[49,50] More mechanistic studies appear to be necessary to understand their low potency. It has been noticed that protein

methyltransferases, though structurally similar in terms of conversed SAM-binding motifs, can display a broad range of affinity to the same ligand (e.g., SAM and sinefungin) and this variation, even between closely related methyltransferases, could not be readily justified according to their static structures.[3,8−10] This observation therefore argues that individual protein methyltransferases may achieve tight interaction with specific ligands by adopting alternative but better matched conformations. Our current success in identifying the *N*-alkyl sinefungin analogues as SETD2 inhibitors presents the utility and power of using privileged scaffolds to probe these distinct conformations in the course of developing PKMT inhibitors. Given that only a limited number of sinefungin analogues and PKMTs are examined here, we envision a promising use of structural variants of sinefungin as structure and chemical probes to elucidate functions of protein methyltransferases.

CONCLUSION

In this work, we outlined an approach, apart from the conventional high-throughput screening, to identify target-specific methyltransferase inhibitors by screening privileged small-molecule scaffolds against diverse methyltransferases. Among the small set of sinefungin derivatives synthesized here, Pr-SNF and *N*-benzyl sinefungin were identified as SETD2-specific inhibitors with decent potency and selectivity. The preferential interaction between the *N*-alkyl sinefungin analogues and SETD2 attributes to the distinct transition-state features of SETD2's catalytically active conformer. With Pr-SNF as a structure probe, we further revealed a dual role of SETD2's post-SET loop on regulating substrate access through a distinct topological reconfiguration. The current work further argues that even closely related SET-domain-containing PKMTs, which contain almost identical SAM-binding motifs, can adopt distinct configurations and thus be selectively inhibited by well-designed small molecules. Although sinefungin was regarded as a pan-inhibitor of methyltransferases, we demonstrated that well-designed sinefungin variants can go beyond the pan-inhibitor category and thus stand as lead compounds for further optimization. Given sinefungin contains rich structural motifs including primary amine, carboxylic acid, adenine and ribosyl moieties and thus can be subject to further derivatization, privileged sinefungin scaffolds are expected to show broad use in the course of developing inhibitors and interrogating functions of methyltransferases.

METHODS

Synthesis and Characterization of Pr-SNF 3c. To a stirred solution of **12c** (0.02 mmol) in methanol (10 mL) was added potassium carbonate (14 mg, 0.1 mmol). The resultant mixture was stirred at ambient temperature for 8 h, concentrated to dryness, and then redissolved in 10 mL water. To the mixture was added hydrazine monohydrate (5 μL, 0.1 mmol). The reaction was stirred for 8 h at ambient temperature, neutralized with 1 M aqueous HCl, and then concentrated under reduced pressure. This mixture was then dissolved in 6 mL ethanol:water (5:1). To this solution was added 20 μL acetic acid and palladium on activated carbon (15 mg, 10 wt %, wet Degussa type). The subsequent hydrogenation reaction was carried out with hydrogen balloon for 12 h. The reaction mixture was filtered through a short pad of Celite and washed out with 20 mL MeOH and then 20 mL 0.1% TFA/water. The combined filtrates were concentrated under reduced pressure. The resultant crude products were purified by preparative reversed-phase HPLC (XBridge Prep C18 5 μm OBD 19 × 150 mm) with 0−15% gradient of acetonitrile in aqueous trifluoroacetic acid (0.1%) in 10 min and a flow rate of 10 mL/min. The fractions containing Pr-SNF were collected. The volatile solvents were removed by SpeedVac. The resultant solution was lyophilized to give the desirable product **3c** with overall 7% from compound **4**. Pr-SNF was dissolved in water and stored at −20 °C before use. The compounds **3a**, **3b**, and **3d** were obtained in a similar manner (Supporting Information).

3a. R = Me, 52% yield. ^{1}H NMR (600 MHz, MeOD): δ 1.96−2.03(m, 2H), 2.05−2.08(m, 2H), 2.25−2.29(m, 2H), 2.64(s, 3H), 3.43−3.45(m, 1H), 3.99−4.03(m, 1H), 4.19−4.22(m, 1H), 4.36(t, 1H, *J* = 5.9 Hz), 4.65(dd, 1H, *J* = 5.4 Hz, 3.7 Hz), 6.01(d, 1H, *J* = 3.7 Hz), 8.35(s, 1H), 8.36(s, 1H); ^{13}C NMR (150 MHz, MeOD): δ 26.54, 27.60, 31.43, 33.55, 53.59, 58.23, 74.86, 75.01, 80.92, 91.85, 117.99(q, *J* = 289.7 Hz), 121.15, 143.44, 149.45, 150.10, 154.64, 162.57(q, *J* = 35.5 Hz),171.52; MS(ESI) *m*/*z*: 396 [M+H]$^+$; HRMS: calcd for $C_{17}H_{28}N_7O_5$ ([M+H]$^+$): 396.1995; found: 396.1982.

3b. R = Et, 56% yield. ^{1}H NMR (600 MHz, MeOD): δ 1.11(t, 3H, *J* = 7.2 Hz), 1.93−1.97(m, 2H), 1.99−2.07(m, 2H), 2.23−2.27(m, 1H), 2.28−2.32(m, 1H), 3.05(q, 2H, *J* = 7.2 Hz), 3.46−3.48(m, 1H), 3.97(t, 1H, *J* = 6.0 Hz), 4.19−4.22(m, 1H), 4.37(t, 1H, *J* = 6.0 Hz), 4.70(dd, 1H, *J* = 5.4 Hz, 3.8 Hz), 5.99(d, 1H, *J* = 3.8 Hz), 8.30(s, 2H); ^{13}C NMR (150 MHz, MeOD): δ 11.53, 26.99, 27.71, 33.51, 41.92, 53.75, 56.89, 74.57, 75.17, 80.91, 91.78, 118.09(q, *J* = 289.2 Hz), 121.12, 142.79, 150.26, 151.64, 156.02, 162.70(q, *J* = 35.4 Hz),171.77 ; MS(ESI) *m*/*z*: 410 [M+H]$^+$; HRMS: calcd for $C_{17}H_{28}N_7O_5$ ([M+H]$^+$): 410.2152; found: 410.2142.

3c. R = Pr, 57% yield. ^{1}H NMR (500 MHz, MeOD): δ 0.83(t, 3H, *J* = 7.4 Hz), 1.42−1.49(m, 1H), 1.52−1.59(m, 1H), 1.94−2.09(m, 4H), 2.21−2.26(m, 1H), 2.29−2.35(m, 1H), 2.92(t, 2H, *J* = 8.0 Hz) 3.44−3.48(m, 1H), 4.01(t, 1H, *J* = 6.0 Hz), 4.19−4.22(m, 1H), 4.40(t, 1H, *J* = 6.0 Hz), 4.67(dd, 1H, *J* = 5.4 Hz, 3.4 Hz), 6.02(d, 1H, *J* = 3.4 Hz), 8.35(s, 1H), 8.36(s, 1H); ^{13}C NMR (150 MHz, MeOD): δ 11.20, 20.77, 27.05, 27.64, 33.32, 48.23, 53.54, 57.29, 74.83, 75.16, 80.91, 91.90, 117.92 (q, *J* = 289.4 Hz),121.11, 143.47, 149.35, 150.09, 154.55, 162.44(q, *J* = 35.8 Hz),171.50; MS(ESI) *m*/*z*: 424 [M+H]$^+$; HRMS: calcd for $C_{18}H_{30}N_7O_5$ ([M+H]$^+$): 424.2308; found: 424.2296.

3d. R = Bn, 30% yield. ^{1}H NMR (600 MHz, MeOD): δ 1.97−2.10(m, 4H), 2.31 (ddd, 1H, *J* = 15.8 Hz, 5.8 Hz, 3.2 Hz), 2.40−2.45(m, 1H), 3.57−3.59(m, 1H), 3.99(t, 1H, *J* = 6.0 Hz), 4.12(d, 1H, *J* = 13.0 Hz), 4.20(d, 1H, *J* = 13.0 Hz), 4.41(t, 1H, *J* = 6.0 Hz), 4.70(dd, 1H, *J* = 5.8 Hz, 4.0 Hz), 5.49(s, 2H), 5.99(d, 1H, *J* = 3.8 Hz), 7.10(d, 2H, *J* = 7.2 Hz), 7.23(t, 2H, *J* = 7.2 Hz), 7.31(t, 1H, *J* = 7.2 Hz), 8.20(s, 1H), 8.33(s, 1H); ^{13}C NMR (150 MHz, MeOD): δ 27.09, 27.87, 32.45, 53.71, 54.96, 57.08, 74.33, 74.84, 80.98, 91.88, 121.22, 130.22, 130.55, 130.68, 132.26, 142.88, 150.14, 151.49, 155.86, 162.55(q, *J* = 35.4 Hz), 171.75; MS(ESI) *m*/*z*: 472 [M+H]$^+$; HRMS: calcd for $C_{22}H_{30}N_7O_5$ ([M+H]$^+$): 472.2308; found: 472.2299.

Protein Expression and Purification for the Assays of Enzymatic Activities. Full-length SET7/9, SET8 (residues 191−395), SETD2 (residues 1347−1711, native and mutants), GLP (residues 951−1235), G9a (residues 913−1193), SUV39H2 (residues 112−410), PRMT1 (residues 10−352), PRMT3 (residues 211−531), and CARM1 (residues 19−608) were expressed and purified as previously reported (see the Supporting Information). DOT1L (residues 1−420), SUV420H1 (residues 69−335), and SUV420H2 (residues 2−248) containing an N-terminal His tag were overexpressed in *E. coli* BL21 (DE3) V2R-pRARE (SGC) and purified by Ni-NTA column (Qiagen). The EZH2 complex containing EZH2 (residues 1−751), EED (residues 1−441), and SUZ12 (residues 1−739) and the MLL complex containing MLL (residues 3745−3969), WDR5 (residues 1−334), and RBBP5 (residues 1−538) were cloned in a pFastBac Dual vector (Invitrogen) with an N-terminal His_6-tag on MLL or EZH2. Both complexes were expressed in SF9 cells and purified by a Ni-NTA column. Additional purification steps were used if needed.

Biochemical Assays of Methylation Activities. Three assays (the filter paper assay, scintillation proximity assay (SPA), and the fiber filterplate assay) were used to determine the activities of methyltransferases according to the readiness of assay reagents and the characters of enzymes. The filter paper assay, in which ^{3}H-Me of

[^{3}H-Me]-SAM is transferred to peptide substrates, followed by filter binding, and then quantification with a scintillation counter, was used to examine the activities of G9a, GLP, SUV39H2, SET7/9, SET8, SETD2 (wild type and mutants), PRMT1, PRMT3, and CARM1. The SPA, in which ^{3}H-Me of [^{3}H-Me]-SAM is transferred to biotinylated substrates, followed by immobilization onto SPA plate and topcount plate reading, was applied to determine the activities of SUV420H1, SUV420H2, EZH2 and MLL complexes, and DNMT1. The fiber filterplate assay, in which ^{3}H-Me of [^{3}H-Me]-SAM is transferred to a protein substrate, followed by acid precipitation, immobilization to fiber filterplate and topcount plate reading, was used for DOT1L. The IC_{50} values were obtained by fitting inhibition percentage versus inhibitor concentration using GraphPad Prism5 or SigmaPlot software.

Crystallization, Data Collection, and Structure Determination (See the SI for Details). Human SETD2 (residues 932−1208) with an N-terminal 6 × histidine tag was overexpressed in *E. coli* BL21 (DE3) codon plus RIL strain (Stratagene) and purified by HiTrap chelating column (GE Healthcare), Superdex200 column (GE Healthcare), and then ion-exchange chromatography. Purified SETD2 protein (10 mg/mL) was complexed with SAM (Sigma), which was degraded into SAH during crystallization, at a 1:10 protein to ligand molar ratio, and crystallized using sitting drop vapor diffusion method. One μL of the protein solution was mixed with 1 μL of the reservoir solution containing 30% PEG 2K MME and 0.1 M KSCN at 20 °C. For the complex of SETD2 with Pr-SNF, the purified SETD2 was incubated with the inhibitor at a 1:5 protein to inhibitor molar ratio and crystallized using a sitting drop vapor diffusion method. Protein solution 1 μL was mixed with 1 μL of reservoir solution containing 20% PEG4000, 10% isopropanol, and 0.1 M HEPES (pH 7.5) at 20 °C. X-ray diffraction data for the SETD2−SAH complex was collected at 100 K at beamline19ID of Advanced Photon Source (APS). The methyltransferase domain structure of SETD2 in complex with SAH was solved by molecular replacement with human SUV39H2 (PDB code 2R3A) as the search model. The SEDT2−SAH structure was subsequently used as model to solve the structure of the Pr-SNF−SETD2 complex. Contoured omission electronic density maps for SAH, Pr-SNF, and the autoinhibitory post-SET loops were simulated to confirm the ligand binding or loop reconfiguration.

Molecular Docking. To compare the SETD2−Pr-SNF complex with SAH-bound SETD2 and other PKMTs, the Pr-SNF ligand was overlaid with the SAM or SAH in complex with the structures of SETD2 (PDB code 4H12), SET8 (PDB code 1ZKK), MLL (PDB code 2W5Z), GLP (PDB code 2RFI), G9a (PDB code 3RJW), SUV39H2 (PDB code 2R3A), SUV420H1 (PDB code 3S8P), and SUV420H2 (PDB code 3RQ4) with ICM version 3.7-2b (Molsoft, San Diego).

Kinetics Analysis. The filter paper assay was used to determine the initial velocities of SETD2 in the presence of varied concentrations of H3 peptide substrate (residues 20−50) and [^{3}H-Me]-SAM cofactor. $K_{m,SAM}$, $K_{m,Substrate}$, and k_{cat} were obtained from the secondary double-reciprocal plots of the initial velocities versus the concentrations of substrate or cofactor according to eqs S1 and S2.[45] The kinetic parameters ($K_{m,SAM}$, $K_{m,Substrate}$, and k_{cat}) were further confirmed upon fitting the same set of initial velocities versus the concentrations of SAM and peptide substrate via nonlinear regression (Figure S1b). To obtain the inhibition constant K_d (K_i) of Pr-SNF on SETD2, the methylation kinetics were measured with the filter paper assay in the presence of varied amounts of the inhibitor. The secondary double-reciprocal plots of the initial velocities versus the concentration of the inhibitor were the generated and further processed according to eqs S3−S6 to give K_d.[45]

■ ASSOCIATED CONTENT

Supporting Information

Reagents, assays, crystallography, molecular docking, synthesis, the full author list of refs 20, 21, and 26, Figures S1−S3, and Tables S1−S3. This material is available free of charge via the Internet at http://pubs.acs.org.

■ AUTHOR INFORMATION

Corresponding Author

jr.min@utoronto.ca; luom@mskcc.org

Author Contributions

⊥These authors contributed equally.

Notes

The authors declare no competing financial interest.

■ ACKNOWLEDGMENTS

The atomic coordinates and structure factors reported in this paper have been deposited in the Protein Data Bank, www.pdb.org (PDB codes 4H12 and 4FMU). This work is supported by Mr. William H. Goodwin and Mrs. Alice Goodwin Commonwealth Foundation for Cancer Research (M.L.), The Experimental Therapeutics Center of Memorial Sloan-Kettering Cancer Center (M.L.), NIGMS (1R01GM096056, M.L.), NINDS (R21NS071520, M.L.), and the Structural Genomics Consortium (J.M.), which is a registered charity (1097737) that receives funds from the Canadian Institutes for Health Research, the Canadian Foundation for Innovation, Genome Canada through the Ontario Genomics Institute, GlaxoSmithKline, Karolinska Institute, The Knut and Alice Wallenberg Foundation, the Ontario Innovation Trust, the Ontario Ministry for Research and Innovation, Merck & Co., the Novartis Research Foundation, the Swedish Agency for Innovation Systems, the Swedish Foundation for Strategic Research, and the Wellcome Trust.

■ REFERENCES

(1) Kouzarides, T. *Cell* **2007**, *128*, 693.
(2) Kouzarides, T. *Cell* **2007**, *128*, 802.
(3) Luo, M. *ACS Chem. Biol.* **2012**, *7*, 443.
(4) Lee, Y. H.; Stallcup, M. R. *Mol. Endocrinol.* **2009**, *23*, 425.
(5) Spannhoff, A.; Hauser, A. T.; Heinke, R.; Sippl, W.; Jung, M. *ChemMedChem* **2009**, *4*, 1568.
(6) Copeland, R. A.; Solomon, M. E.; Richon, V. M. *Nat. Rev. Drug Discov.* **2009**, *8*, 724.
(7) Min, J.; Feng, Q.; Li, Z.; Zhang, Y.; Xu, R. M. *Cell* **2003**, *112*, 711.
(8) Richon, V. M.; Johnston, D.; Sneeringer, C. J.; Jin, L.; Majer, C. R.; Elliston, K.; Jerva, L. F.; Scott, M. P.; Copeland, R. A. *Chem. Biol. Drug Des.* **2011**, *78*, 199.
(9) Campagna-Slater, V.; Mok, M. W.; Nguyen, K. T.; Feher, M.; Najmanovich, R.; Schapira, M. *J. Chem. Inf. Model* **2011**, *51*, 612.
(10) Schapira, M. *Curr. Chem. Genomics* **2011**, *5*, 85.
(11) Daigle, S. R.; Olhava, E. J.; Therkelsen, C. A.; Majer, C. R.; Sneeringer, C. J.; Song, J.; Johnston, L. D.; Scott, M. P.; Smith, J. J.; Xiao, Y.; Jin, L.; Kuntz, K. W.; Chesworth, R.; Moyer, M. P.; Bernt, K. M.; Tseng, J.-C.; Kung, A. L.; Armstrong, S. A.; Copeland, R. A.; Richon, V. M.; Pollock, R. M. *Cancer Cell* **2011**, *20*, 53.
(12) Yao, Y.; Chen, P.; Diao, J.; Cheng, G.; Deng, L.; Anglin, J. L.; Prasad, B. V. V; Song, Y. *J. Am. Chem. Soc.* **2011**, *133*, 16746.
(13) Greiner, D.; Bonaldi, T.; Eskeland, R.; Roemer, E.; Imhof, A. *Nat. Chem. Biol.* **2005**, *1*, 143.
(14) Kubicek, S.; O'Sullivan, R. J.; August, E. M.; Hickey, E. R.; Zhan, Q.; Teodoro, M. L.; Rea, S.; Mechtler, K.; Kowalski, J. A.; Homon, C. A.; Kelly, T. A.; Jenuwein, T. *Mol. Cell* **2007**, *25*, 473.
(15) Ferguson, A. D.; Larsen, N. A.; Howard, T.; Pollard, H.; Green, I.; Grande, C.; Cheung, T.; Garcia-Arenas, R.; Cowen, S.; Wu, J.; Godin, R.; Chen, H.; Keen, N. *Structure* **2011**, *19*, 1262.
(16) Gutierrez, J. A.; Luo, M.; Singh, V.; Li, L.; Brown, R. L.; Norris, G. E.; Evans, G. B.; Furneaux, R. H.; Tyler, P. C.; Painter, G. F.; Lenz, D. H.; Schramm, V. L. *ACS Chem. Biol.* **2007**, *2*, 725.
(17) Schramm, V. L. *Annu. Rev. Biochem.* **2011**, *80*, 703.
(18) Horowitz, S.; Yesselman, J. D.; Al-Hashimi, H. M.; Trievel, R. C. *J. Biol. Chem.* **2011**, *286*, 18658.

(19) Zhang, X. D.; Bruice, T. C. *Biochemistry* **2008**, *47*, 2743.
(20) Zhang, J.; Ding, L.; Holmfeldt, L.; et al. *Nature* **2012**, *481*, 157.
(21) Varela, I.; Tarpey, P.; Raine, K.; et al. *Nature* **2011**, *469*, 539.
(22) Newbold, R. F.; Mokbel, K. *Anticancer Res.* **2010**, *30*, 3309.
(23) Hu, M.; Sun, X. J.; Zhang, Y. L.; Kuang, Y.; Hu, C. Q.; Wu, W. L.; Shen, S. H.; Du, T. T.; Li, H.; He, F.; Xiao, H. S.; Wang, Z. G.; Liu, T. X.; Lu, H.; Huang, Q. H.; Chen, S. J.; Chen, Z. *Proc. Natl. Acad. Sci. U.S.A.* **2010**, *107*, 2956.
(24) Duns, G.; van den Berg, E.; van Duivenbode, I.; Osinga, J.; Hollema, H.; Hofstra, R. M.; Kok, K. *Cancer Res.* **2010**, *70*, 4287.
(25) de Almeida, S. F.; Grosso, A. R.; Koch, F.; Fenouil, R.; Carvalho, S.; Andrade, J.; Levezinho, H.; Gut, M.; Eick, D.; Gut, I.; Andrau, J. C.; Ferrier, P.; Carmo-Fonseca, M. *Nat. Struct. Mol. Biol.* **2011**, *18*, 977.
(26) Dalgliesh, G. L.; Furge, K.; Greenman, C.; et al. *Nature* **2010**, *463*, 360.
(27) Nimura, K.; Ura, K.; Shiratori, H.; Ikawa, M.; Okabe, M.; Schwartz, R. J.; Kaneda, Y. *Nature* **2009**, *460*, 287.
(28) Kuo, A. J.; Cheung, P.; Chen, K.; Zee, B. M.; Kioi, M.; Lauring, J.; Xi, Y.; Park, B. H.; Shi, X.; Garcia, B. A.; Li, W.; Gozani, O. *Mol. Cell* **2011**, *44*, 609.
(29) Morishita, M.; di Luccio, E. *Biochim. Biophys. Acta* **2011**, *1816*, 158.
(30) Pasillas, M. P.; Shah, M.; Kamps, M. P. *Hum. Mutat.* **2011**, *32*, 292.
(31) Cross, N. C. *Oncotarget* **2012**, *3*, 3.
(32) Yang, P.; Guo, L.; Duan, Z. J.; Tepper, C. G.; Xue, L.; Chen, X.; Kung, H. J.; Gao, A.; Zou, J. X.; Chen, H. W. *Mol. Cell. Biol.* **2012**, *32*, 3121.
(33) Ghosh, A. K.; Liu, W. *J. Org. Chem.* **1996**, *61*, 6175.
(34) Dubber, M.; Lindhorst, T. K. *Synthesis* **2001**, 327.
(35) Sun, J.; Dong, Y.; Cao, L.; Wang, X.; Wang, S.; Hu, Y. *J. Org. Chem.* **2004**, *69*, 8932.
(36) Yin, X.; Zhao, G.; Schneller, S. W. *Tetrahedron Lett.* **2007**, *48*, 4809.
(37) Baldwin, J. E.; Adlington, R. M.; Mitchell, M. B. *Tetrahedron* **1995**, *51*, 5193.
(38) Qian, C.; Zhou, M. M. *Cell. Mol. Life Sci.* **2006**, *63*, 2755.
(39) Cheng, X. D.; Collins, R. E.; Zhang, X. *Annu. Rev. Biophys. Biomol. Struct.* **2005**, *34*, 267.
(40) An, S.; Yeo, K. J.; Jeon, Y. H.; Song, J. J. *J. Biol. Chem.* **2011**, *286*, 8369.
(41) Morishita, M.; di Luccio, E. *Biochem. Biophys. Res. Commun.* **2011**, *412*, 214.
(42) Qiao, Q.; Li, Y.; Chen, Z.; Wang, M.; Reinberg, D.; Xu, R. M. *J. Biol. Chem.* **2011**, *286*, 8361.
(43) Wu, H.; Min, J. R.; Lunin, V. V.; Antoshenko, T.; Dombrovski, L.; Zeng, H.; Allali-Hassani, A.; Campagna-Slater, V.; Vedadi, M.; Arrowsmith, C. H.; Plotnikov, A. N.; Schapira, M. *PLoS One* **2010**, *5*, e8570.
(44) Krishnan, S.; Horowitz, S.; Trievel, R. C. *ChemBioChem* **2011**, *12*, 254.
(45) Segel, I. H. *Enzyme Kinetics: Behavior and Analysis of Rapid Equilibrium and Steady-State Enzyme Systems*; John Wiley & Sons, Inc.: Hoboken, NJ, 1993.
(46) Edmunds, J. W.; Mahadevan, L. C.; Clayton, A. L. *Embo J.* **2008**, *27*, 406.
(47) Wagner, E. J.; Carpenter, P. B. *Nat. Rev. Mol. Cell Biol.* **2010**, *13*, 115.
(48) Li, Y.; Trojer, P.; Xu, C. F.; Cheung, P.; Kuo, A.; Drury, W. J., 3rd; Qiao, Q.; Neubert, T. A.; Xu, R. M.; Gozani, O.; Reinberg, D. *J. Biol. Chem.* **2009**, *284*, 34283.
(49) t Hart, P.; Lakowski, T. M.; Thomas, D.; Frankel, A.; Martin, N. I. *ChemBioChem* **2011**, *12*, 1427.
(50) Mori, S.; Iwase, K.; Iwanami, N.; Tanaka, Y.; Kagechika, H.; Hirano, T. *Bioorg. Med. Chem. Lett.* **2010**, *18*, 8158.